Reprinted from

Comments on Condensed Matter Physics

Physics of the *Artificial Atoms*: Quantum Dots in a Magnetic Field

by

TAPASH CHAKRABORTY

GORDON AND BREACH SCIENCE PUBLISHERS

NEW YORK ● LONDON ● PARIS ● MONTREUX ● TOKYO ● MELBOURNE

Physics of the *Artificial Atoms*: Quantum Dots in a Magnetic Field

Rapid advances in submicron technology have led to the fabrication of quasi-zero-dimensional electron systems which allow us to study the physics of a few-electron system under quantum confinement and in a magnetic field. The purpose of this review is to discuss the experimental and theoretical information currently available in the literature on this system. We also highlight current trends in the field and point out some of the questions which need to be answered.

I. INTRODUCTION

Quantum dots (quasi-zero-dimensional electron systems) are one of the most interesting systems in semiconductor nanostructures and have received considerable attention recently.[1,2] With today's rapid advances in microfabrication technology, it has been possible to confine laterally the two-dimensional electron system (2DES) into dots of diameters below 100 nm. Since the mean free path of electrons at low temperatures is larger than this width, transport and optical properties of the electron systems in the dot should exhibit quasi-zero-dimensional behavior. Each dot typically contains between 1 and 200 electrons. These quantum confined few-electron systems are often referred to as *artificial atoms* where the potential of the nucleus is replaced by an artificially created potential.

Besides being an interesting physical system where new physical

Comments Cond. Mat. Phys.
1992, Vol. 16, No. 1, pp. 35–68
Reprints available directly from the publisher
Photocopying permitted by license only

phenomena are expected to be explored, a quantum dot is also interesting from a technological point of view. As the author of Ref. 2 pointed out, *the interest arises on both the primary (new device concepts) and the secondary (impact on existing devices) levels. The tools for nanostructure fabrication are the staples of the semiconductor industry and thus the connection is direct.*

The scope of this Comment is to review the current scientific literature on the fascinating field of zero-dimensional systems in a magnetic field. I shall focus mostly on magnetocapacitance measurements and optical experiments on quantum dots and their theoretical interpretation, but transport measurements and the associated theoretical work will also be briefly discussed.

II. EXPERIMENTAL WORK

A. Capacitance Studies

The density of states of the discrete energy levels in quantum dots as a function of the gate voltage and an applied magnetic field perpendicular to the heterojunction interface was measured by Hansen *et al.*[3] via capacitance spectroscopy. In these experiments the samples are modulation-doped GaAs/AlGaAs heterostructure capacitors, grown on conducting n^+ substrates which serve as electrodes. Electrons are confined at the GaAs/AlGaAs interface. The lateral confinement results from the band bending beneath the etched regions that separate adjacent dots.

Figure 1 shows the gate voltage derivative of the capacitance as a function of the gate voltage at different magnetic fields. The peaks at positive gate voltages show complicated behavior even at very low magnetic fields ($B < 0.2$ T). However, as the field is increased to about $B = 1$ T one can clearly distinguish the peak shifts and splitting of many of the peaks. At higher fields, some of the peaks increase in size with other, weaker peaks moving between them. The stronger peaks are the precursors to Landau levels which the smaller peaks join as the field increases and increase their degeneracy.[3] The peak positions are plotted as a function of the magnetic field in Fig. 1b. The stronger peaks that become Landau levels at high magnetic fields are plotted as solid

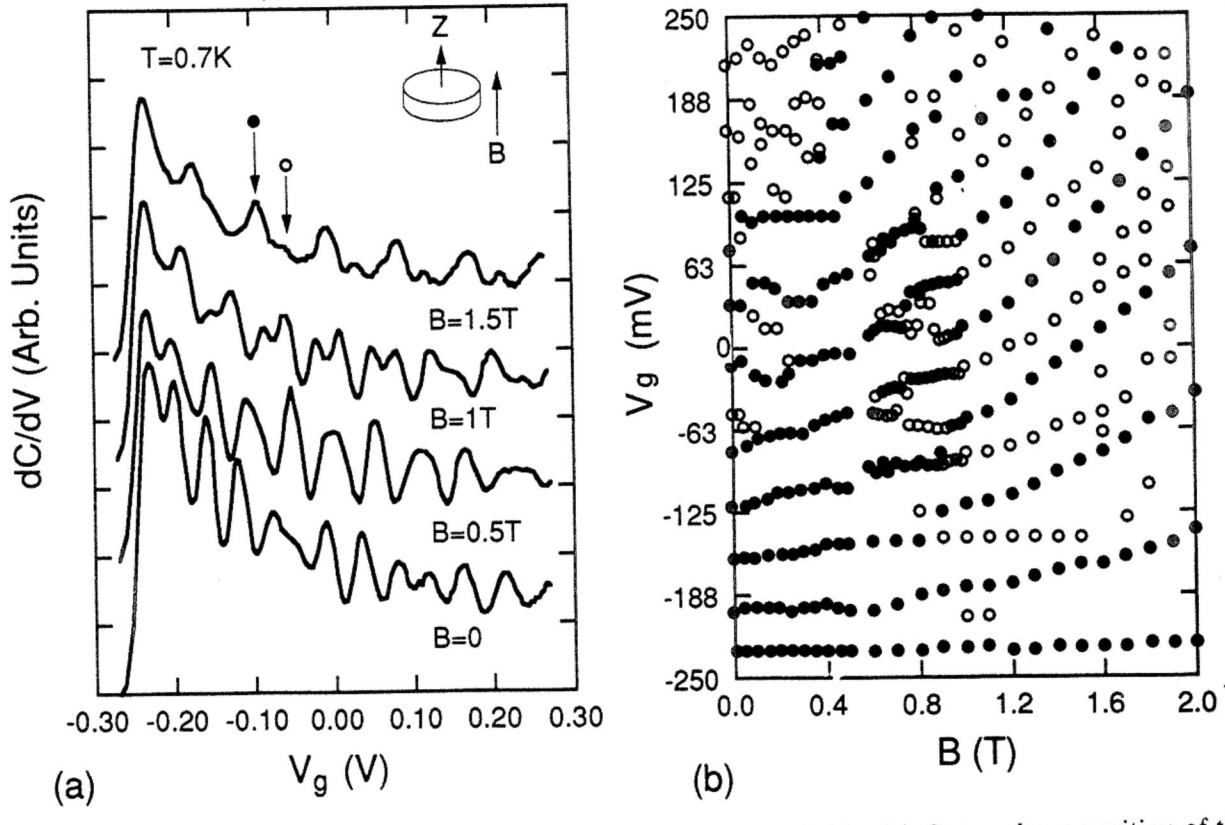

FIGURE 1 (a) Capacitance spectra for 300 nm quantum dots at various magnetic fields. (b) Gate voltage position of the peaks (Ref. 3).

dots while the weak peaks are shown by open dots. The oscillatory structure in the capacitance as shown in Fig. 1a can be attributed to the discrete energy levels of a quantum dot indicating that the quantization has been achieved in all directions. The splitting of the peaks is believed to occur due to the interplay between competing spatial and magnetic quantization.

Another interesting result in capacitance spectroscopy is the observation by Hansen *et al.*[4] of fractionally quantized states, familiar from the fractional quantum Hall effect in a two-dimensional electron system.[5] For dots containing about 30 electrons in a very high magnetic field, the derivative of the capacitance vs. the gate voltage shows downward cusps at 1/3 and 2/3 filling factors (Fig. 2a). The temperature dependence of the minima (Fig. 2b) at these two filling factors is also consistent with that of the fractional quantum Hall states.

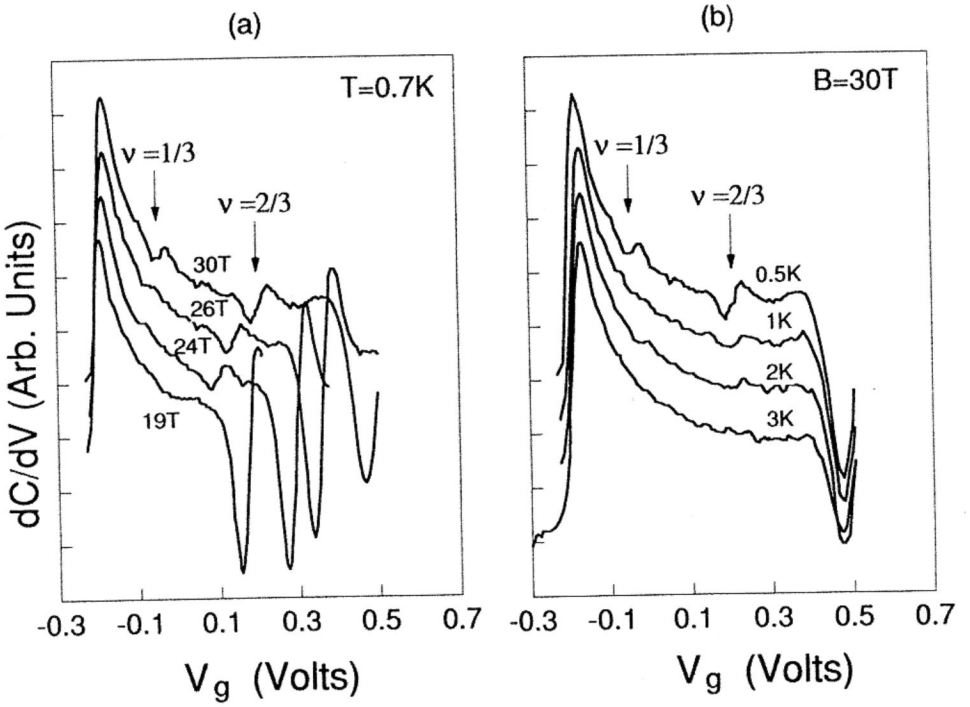

FIGURE 2 (a) Derivative of the capacitance vs. the gate voltage for a sample with 3000 Å dots. (b) Temperature dependence of the fractional states at $B = 30$ T (Ref. 4).

B. Optical Studies

The first magneto-optical experiments on quantum dots were performed by Merkt *et al.*[1,6] using a metal-oxide-semiconductor (MOS) structure with the alloy NiCr evaporated onto the InSb substrate as a Schottky barrier. The dot array was prepared by holographic lithography, details of which can be found in Refs. 1 and 6. Figure 3a shows a schematic picture of the lateral band structure across the dots created in this arrangement. The Fermi energy E_F is pinned at the NiCr/InSb interface above the valence band edge. Under the small dot areas where there is no metal on the InSb surface, mobile inversion electrons are induced by a gate voltage V_g. There is virtually no tunneling between the adjacent dots since the barrier height between the dots is of the order of the band gap energy (E_g = 236 meV) and the distance is of the order of the period (a = 250 nm) of the dot array. The conduction band edge near a minimum is approximately that of a harmonic oscillator well of characteristic frequency ω_0.

The average number n_0 of electrons in a dot was estimated from the cyclotron resonances in strong magnetic fields and the spectroscopy of the dots was carried out with linearly polarized far-infrared (FIR) laser light. Figure 3b shows the most interesting results obtained by these authors. The measured resonant frequency is found to be independent of electron number (inset). These resonances are, in fact, related to single-particle transition energies in a bare confinement potential (see Section IIIA). A possible explanation is available in Section IIID.

Two examples of the dot structures created by Heitmann *et al.*[7,8] are shown in Fig. 4. They were prepared from modulation-doped AlGaAs/GaAs heterostructures. For the *deep-mesa-etched* quantum dots in Fig. 4a an array of photoresist dots (with a period of a = 1000 nm both in x- and y-directions) was created by a holographic double exposure. Employing anisotropic plasma etching, rectangular 200 nm deep grooves were etched all the way through the 10 nm thick GaAs cap layer, the 53 nm thick Si-doped AlGaAs layer, and the 23 nm thick undoped AlGaAs spacer layer into the active GaAs. This gives quadratic dots with rounded corners and geometrical dimensions of about 600 × 600 nm.[2] Figure 4b depicts

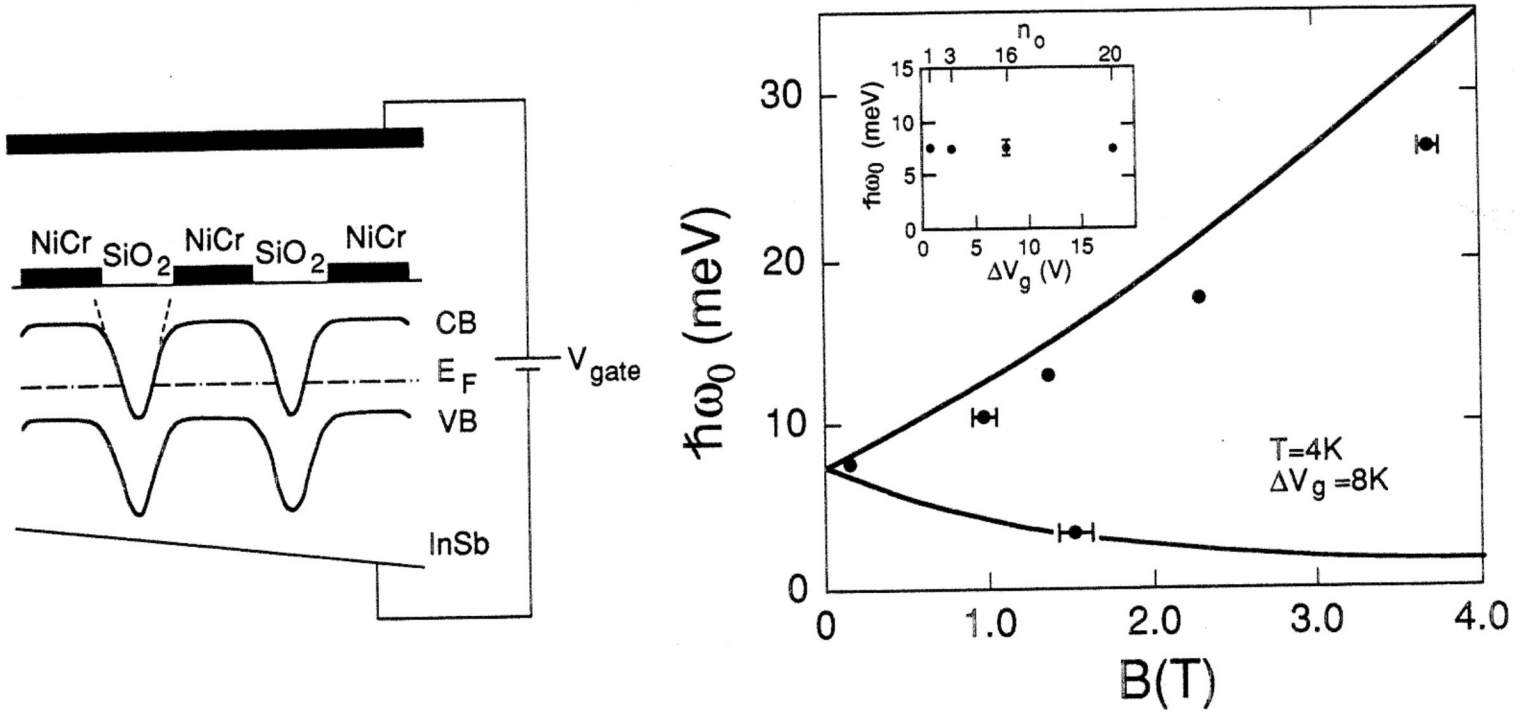

FIGURE 3 (a) Schematic cross-section of the microstructured field-effect device in InSb with its lateral band structure. (b) Zeeman splitting of resonance position in quantum dots. Inset: dependence of resonance energy $\hbar\omega_0$ on voltage ΔV_g and electron number n_0. The solid lines are from the theoretical result Eq. (1) (Refs. 1 and 6).

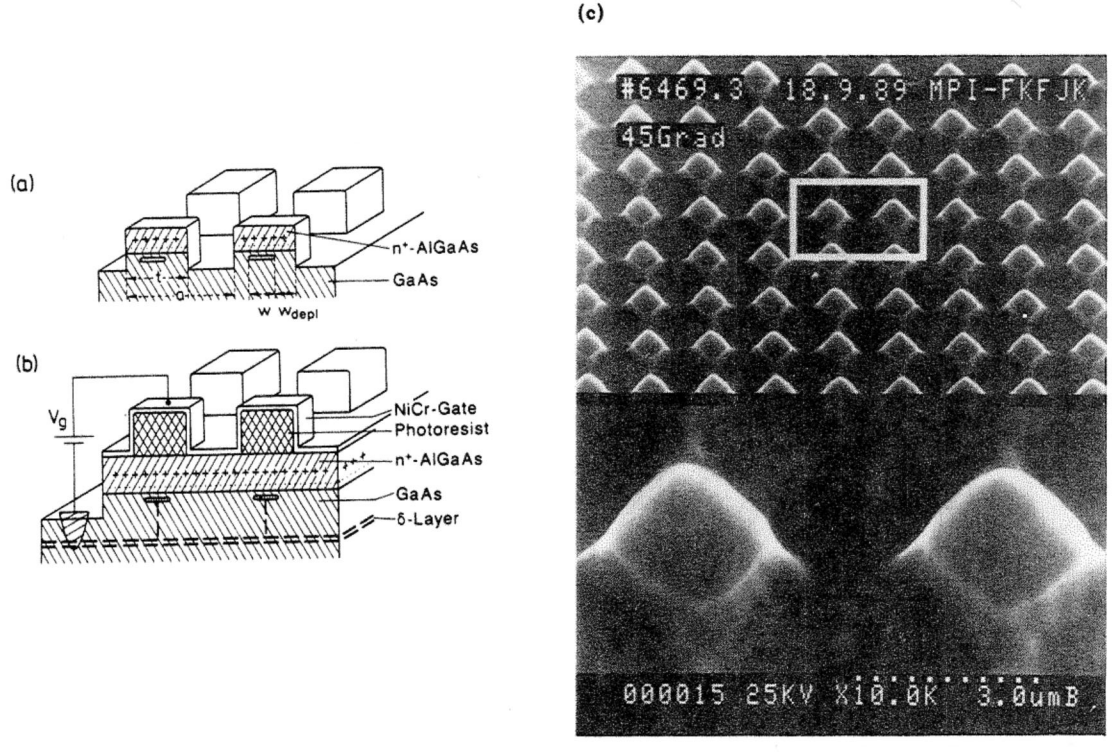

FIGURE 4 Sketch of deep-mesa-etched (a) and field-effect confined (b) quantum dot arrays. (c) Electron micrograph of an array of quantum dots with geometrical dimensions of 600 × 600 nm (Ref. 8).

the split-gate configuration where the channel carriers are depleted via a gate voltage and a varying distance between a NiCr-gate, leaving isolated quantum dots. Variation of the gate distance is achieved via a modulated photoresist layer. A Si δ-doped layer serves as a backcontact to vary the number of electrons in the dot. This δ-layer has a low concentration and impedance such that it is semitransparent for FIR radiation.

The FIR spectra, for a sample with an average of 210 electrons per dot, are shown in Fig. 5a. The transmission $T(B)$ of unpolarized FIR radiation through the sample was measured at fixed magnetic fields B, perpendicular to the surface of the sample. The spectra were normalized to a spectrum $T(B_0)$ with a flat response. The active sample area was 3×3 mm^2 containing 10^7 dots. At $B = 0$ one resonance is observed at $\omega_{01} = 32$ cm^{-1}. With increasing B the resonance splits into two resonances: ω_{1-} decreases in frequency, while the other, ω_{1+}, increases. The dispersion is similar to that observed by Merkt *et al.* For $B \gtrsim 4$ T, a second resonance ω_{2+} was resolved. Figures 5b and 5c show the resonance position for the dots with different electron number. An interesting observation is the resonant anticrossing at $\omega \approx 1.4\omega_{01}$.

This group has also prepared quantum dot structures in InGaAs by deep mesa etching.[9] Massive dots containing 600 electrons were created and found to have an energy spacing of 1 meV. The FIR response for this system showed, in addition to the usual modes, weak additional modes and anticrossing behavior.

More recently, Heitmann *et al.*[10] prepared field-effect confined quantum dot arrays with a well defined number of electrons in each dot, $N = 1, 2, 3$ and 4. The FIR transmission experiment on such dot-arrays (Fig. 4b) revealed an interesting stepwise increase of the integrated absorption strength as a function of the gate voltage. This indicates the incremental charging of each of the 10^8 dots of the array with 1, 2, 3, etc. electrons. This is a remarkable experimental achievement which should enable us in the future to compare the theoretical work on the few-electron system directly with the experiments.

Finally, Lorke *et al.*[11] reported on the electrostatic generation of quantum dots where the coupling strength between dots can be tuned by an applied gate voltage. FIR transmission spectra showed that for strongly coupled dots, new spectral features develop: an

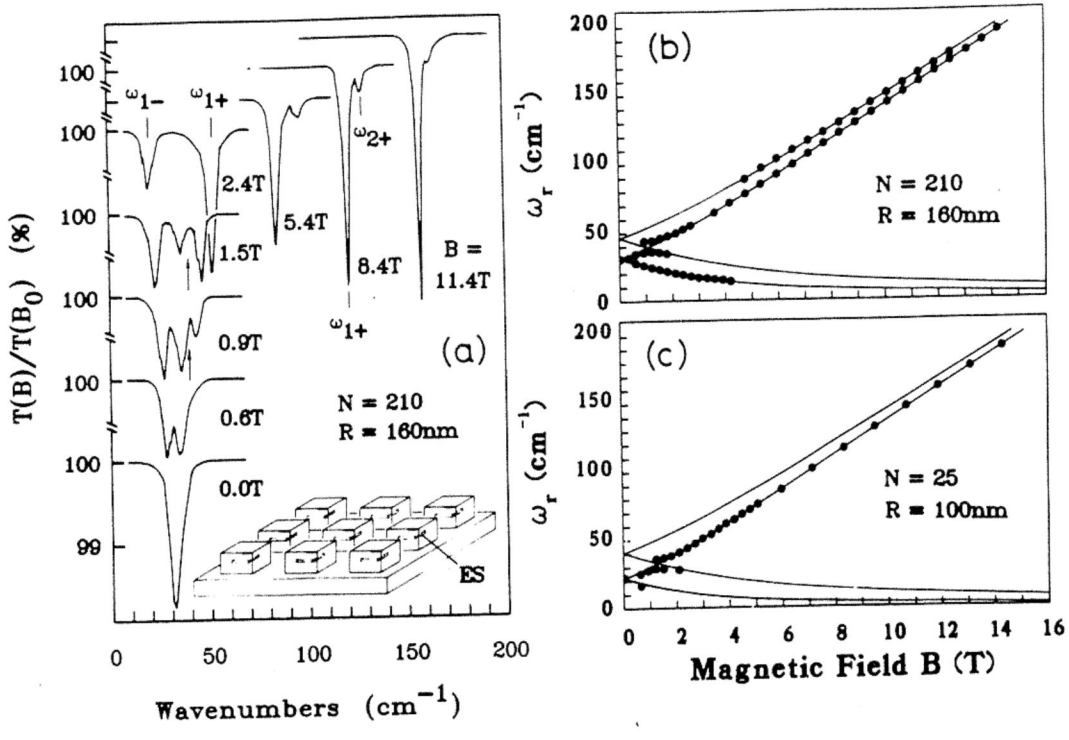

FIGURE 5 (a) Normalized transmission of unpolarized FIR radiation for a AlGaAs–GaAs quantum dot structure with 210 electrons per dot. At $\omega \approx 40\ \text{cm}^{-1}$ ($\uparrow$) there is a pronounced anticrossing intersection. The inset shows the dot structure schematically. In (b) and (c) are shown the experimental B dispersions of resonant absorption in quantum dot structures with 210 and 25 electrons per dot, respectively. The solid lines are theoretical results from Refs. 7 and 8.

additional mode appears at frequencies lower than ω_- and the ω_+ mode branches into two modes at higher magnetic fields.

C. Transport Studies

Excellent reviews exist on transport properties in semiconductor nanostructures.[12,13] In the following, I shall discuss briefly transport measurements by three groups. The Dutch group[14] prepared the dot by creating a disk in a 2DES. This is done by fabricating two pairs A and B (Fig. 6) of metallic gates. A negative voltage of -0.2 V on both gate pairs depletes the electron gas underneath the gates and a quantum dot of diameter 1.5 μm is formed in the 2DES. The narrow channels between the gate pairs are pinched off at this gate voltage. The disk is connected to the wide 2DES regions by two 300 nm wide quantum point contacts (QPC).

In studying zero-dimensional states, this group employed the fact that edge channels are formed when a high magnetic field is applied perpendicular to the 2DES[15] and that electron transport in edge channels is known to be one-dimensional. In high magnetic fields QPCs can thus be used as selective transmitters of edge channels. The zero-dimensional state is obtained by confining a one-dimensional edge channel in a quantum dot between two partially transmitting barriers (Fig. 6). Discrete zero-dimensional states are formed by the constructive interference of electron waves moving along the edge channels. Resonant transmission through the zero-dimensional states was indicated by pronounced oscillations in the conductance with maxima occurring whenever the energy of a zero-dimensional state coincided with the Fermi energy.

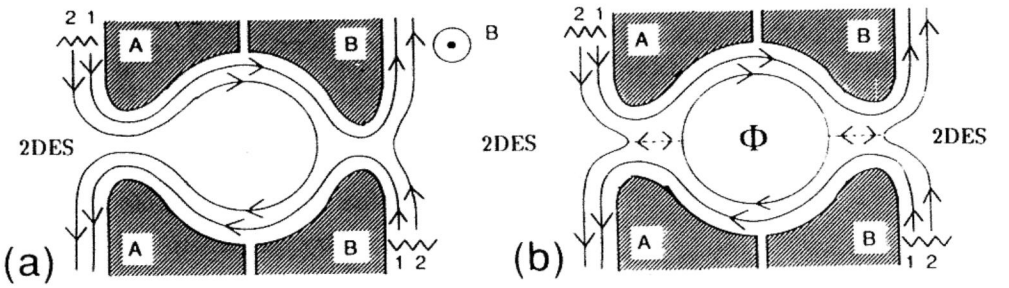

FIGURE 6 Schematic layout of the quantum dot. The edge channels in a high magnetic field are also shown. (a) Adiabatic transport for unequal QPCs A and B. (b) Formation of a one-dimensional loop when an edge channel is only partially transmitted by both QPCs (Ref. 14).

Magnetotransport measurements through quantum dot systems have also been performed by the NRC group.[16] They observed resonant tunneling through the single-electron states of the quantum dot from one edge of the sample to the other. Low and high field magnetotransport measurements through two quantum dots coupled in series were also reported by these authors.

Recently, some very interesting transport measurements in quantum dots were reported by McEuen *et al.*[17] (the MIT group). Their system is shown in Fig. 7a. As above, the electrostatic gates are used to confine and adjust the density of the 2DES. A negative voltage applied to a lithographically patterned split upper gate defines the dot while a positive bias applied to a lower gate adjusts the electron density. The conductance G as a function of gate voltage V_g shows a periodic series of sharp peaks shown in the inset of Fig. 8. The basic periodicity of the peaks can be explained by the standard *Coulomb-blockade* model of single-electron tunneling through a quantum dot[13,17,18]: At low temperatures and infinitesimal applied bias the probability of the dot containing a particular integer charge is close to unity for most values of gate voltage. This is because adding another electron costs a large charg-

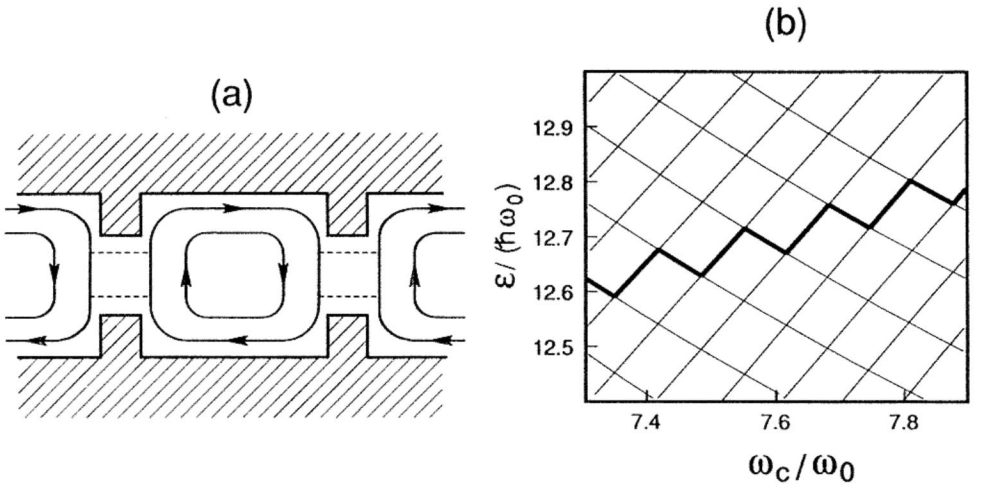

FIGURE 7 Schematic layout of the quantum dot arrangement of McEuen *et al.* (Ref. 17) showing the path of the edge states associated with the lowest two Fock–Darwin levels (FDL). (b) Energy levels of a parabolic quantum dot in a magnetic field. The thick line indicates the energy of the single-particle state that is 78-th lowest in energy. In each period of the sawtooth a single electron is transferred from the second FDL (rising line) to the first FDL (descending line).

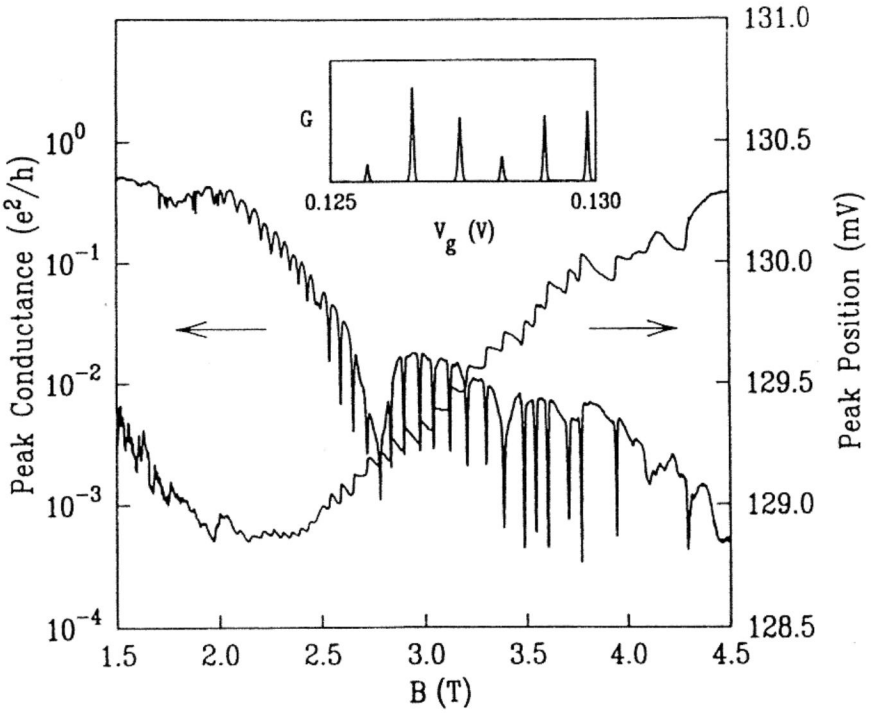

FIGURE 8 Height and position of a conductance peak as a function of the magnetic field. Inset: Conductance vs. V_g at $B = 3$ T (Ref. 17).

ing energy U (the electrostatic energy associated with the incremental charging of the dot by single electrons). As the charge does not fluctuate, transport is suppressed and the conductance is essentially zero. At the gate voltage corresponding to the conductance peaks, however, the energy cost of adding one electron is zero, i.e., the peaks occur when

$$F(N + 1) - F(N) = E_F$$

where $F(N)$ is the free energy of the dot and E_F is the Fermi energy. The probabilities of having N or $N + 1$ electrons on the dot are then both finite and transport proceeds via the fluctuation of the charge on the dot between N and $N + 1$ electrons.

The main result of Fig. 8 is, of course, that with increasing B the height and position of a particular peak behaves in a striking fashion. In the region between 2.5 and 4 T the peak height is periodically suppressed by as much as an order of magnitude. The peak positions show oscillations commensurate with these dips. In

this magnetic field regime two Fock–Darwin levels (FDL) (defined in Section IIIA) are occupied in the dots as shown in Fig. 7b. Theoretically, from the above equation it follows that the condition for the oscillation of the conductance peak is directly related to the behavior [13,18] of the N-th single-particle energy level $\mathscr{E}_N$. The thick line in Fig. 7b shows the behavior of $\mathscr{E}_N$. As the magnetic field is increased, the N-th electron alternately occupies a state in the first FDL and a state in the second FDL. Accordingly, the measured shift of the peak position with B can be related to the shift in $\mathscr{E}_N$. Assuming that the Coulomb energy is constant in the magnetic field range studied, a single-electron energy spectrum was mapped out from the measured peak position (Fig. 9) and was found to be remarkably similar to that obtained theoretically (see Section IIIA). There are, of course, notable deviations from the

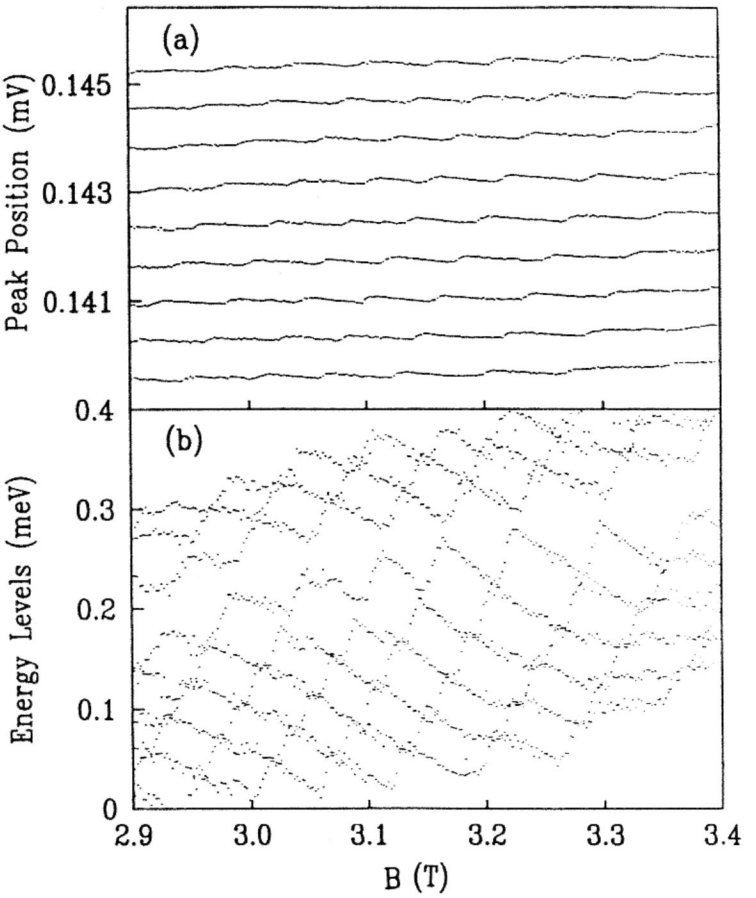

FIGURE 9 (a) Peak position vs. the magnetic field for a series of consecutive peaks. (b) Single-electron energy level spectrum as obtained from (a) (Ref. 17).

theoretical single-electron energy levels such as the discontinuity in the spectrum near 0.2 meV. The spectrum is also not very well reproduced in the higher end of the magnetic field range.

It is quite surprising that a transport measurement on a fairly complicated quantum dot structure can reproduce the energy levels of an ideal parabolic quantum dot. Theories need to be developed to understand the deviations in the inferred spectrum from the theoretically derived spectrum, as well as the validity of the assumptions employed such as the constant-Coulomb-energy model. One interesting point to note is that occupation of the second FDL is quite crucial in interpreting the above results. In the lowest FDL there is no *sawtooth* behavior because no level crossings occur, and for more than two FDL the simple oscillations will be replaced by more complicated behavior. As we shall see in Section IVC, similar sawtooth behavior may be obtained in a quantum *ring* when only the lowest FDL is occupied.

III. THEORETICAL WORK

In order to understand the experimental results discussed above, the first step is to understand the nature of the confining potential and the electronic properties of a single electron in a confining potential in the presence of a magnetic field. The first theoretical work in that direction was by Kumar *et al.*[19] They considered a model of a single quantum dot from the array of dots used in the experiments of Hansen *et al.*[3] The shape of the dot was considered to be rectangular. These authors then solved the Schrödinger and Poisson equations self-consistently within the Hartree approximation, i.e., exchange and correlation effects were neglected. They found that the confining potential has nearly circular symmetry despite the rectangular geometry of the dot system. For seven electrons per dot they also found that the evolution of the energy levels with increasing magnetic field is similar to that found for a parabolic potential.

A. Single-Electron Results

The problem of a single ideally two-dimensional electron, in a circular dot, confined by a parabolic potential $\frac{1}{2}m^*\omega_0^2 r^2$ (m^* is the

electron effective mass) in the presence of an external magnetic field was solved more than half a century ago by Fock[20] (and later by Darwin[21]). It is interesting to note that the same problem (but for zero confinement potential) was studied two years after Fock's work by Landau,[22] leading to the term *Landau levels*.

The single-electron energies

$$\mathscr{E}_{nl} = (2n + |l| + 1)\,\hbar\Omega - \frac{1}{2}\,l\hbar\omega_c \tag{1}$$

depend on the two quantum numbers $n = 0, 1, 2, \ldots$ and $l = 0, \pm 1, \pm 2, \ldots$. Here $\omega_c = eB/m^*c$ is the cyclotron frequency, and $\Omega = (\frac{1}{4}\omega_c^2 + \omega_0^2)^{1/2}$. In the limit, $\omega_0 \to 0$, we have $\mathscr{E} = (\mathcal{N} + 1/2)\,\hbar\omega_c$ where the *Fock–Darwin level* (FDL) index is $\mathcal{N} = n + \frac{1}{2}(|l| - l)$. These energies are plotted in Fig. 10 as a function of the magnetic field. Without the confining potential the energies of the positive l states would be independent of l, but in its presence

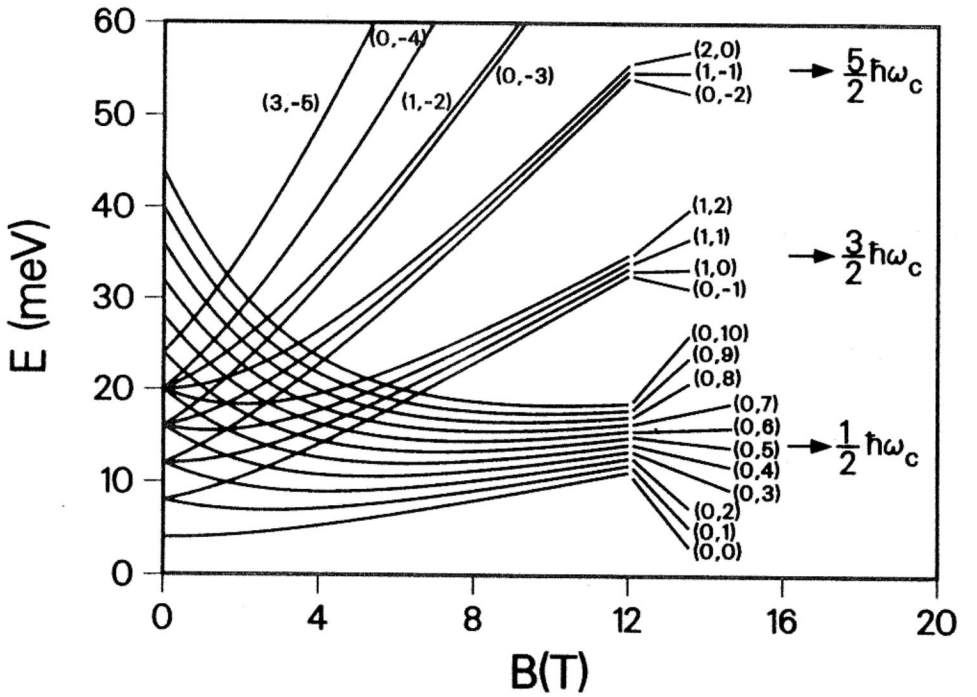

FIGURE 10 Single-electron energy levels in a parabolic dot as a function of the magnetic field. The levels are indicated by their quantum numbers (n, l). The confinement energy is $\hbar\omega_0 = 4$ meV.

they increase with l. For very large B ($\omega_c >> \omega_0$) and for $n = 0$, $l \geq 0$, we get $\mathscr{E} = \frac{1}{2}\hbar\omega_c$, while for $n = 1$, $l \geq 0$, $\mathscr{E} = \frac{3}{2}\hbar\omega_c$, etc. States with $l < 0$ have much higher energies than those for $l > 0$ (Fig. 10). The single-particle wave function is $\phi_{nl} = r^{|l|} \exp(-il\theta) L_n^{|l|}(r^2/2a^2)\exp(-r^2/4a^2)$, where the effective magnetic length is $a = (\hbar/2m^*\Omega)^{1/2}$, $-l$ is the angular momentum quantum number and $L_n(y)$ is the Laguerre polynomial of degree n. As discussed in Section IIC, transport measurements on quantum dots by the MIT group have been able to map these energy levels from the oscillations of the conductance as a function of the magnetic field.

Optical Transitions: Selection Rules

The transition probability $(n, l) \rightleftharpoons (n', l')$ is proportional to the square of the interaction energy.[23] For the interaction between the applied electric field **E** and the electric dipole moments of the electrons, the transition amplitude is

$$A_{nl}^{n'l'} = \langle \phi_{nl} | re^{\pm i\theta} | \phi_{n'l'} \rangle,$$

with the associated oscillator strength

$$f_{nl}^{n'l'} = \frac{2m}{\hbar}\,\omega_{nl}^{n'l'} |A_{nl}^{n'l'}|^2,$$

where $\omega_{nl}^{n'l'} = (\mathscr{E}_{n'l'} - \mathscr{E}_{nl})/\hbar$ is the transition frequency. Using the single-electron wave function in a parabolic confinement, an integral over θ gives $\Delta l = l' - l = \pm 1$ for the allowed transitions. The final result is

$$A_{nl}^{n'l'} = \delta_{n',n}\delta_{l',l\pm1}\left(\frac{2\hbar}{m^*\omega_0}\right)^{1/2}\sqrt{n + |l| + 1}$$

$$- \delta_{n',n+1}\delta_{l',l\pm1}(1 - \delta_{l,0})\left(\frac{2\hbar}{m^*\omega_0}\right)^{1/2}\sqrt{n+1},$$

which leads to $\Delta n = 0, 1$. The corresponding energies are

$$\Delta E_{\pm} = \frac{1}{2}\hbar\,[\omega_0^2 + 4\omega_0^2]^{1/2} \pm \frac{1}{2}\hbar\omega_c = \hbar\Omega \pm \frac{1}{2}\hbar\omega_c \qquad (2)$$

where the + (−) sign corresponds to left (right) circular polarization. Note that with increasing magnetic field, ΔE_+ approaches the cyclotron energy $\hbar\omega_c$, while ΔE_- decreases with the magnetic field. The magneto-optical experiments discussed in Section IIB have in fact observed these two modes of dispersion [see Figs. 3(b) and 5(b)–(c)].

B. Effects of Electron–Electron Interactions

All the experimental results on quantum dots discussed in Section II seem to show predominantly single-electron behavior. As the dots contain more than one electron in most of the cases, the question of the effect of electron–electron interaction still remains to be studied. In the absence of a magnetic field, Bryant[24] has shown that the electron–electron interaction has a significant influence on the energy spectrum of quantum microstructures.

A detailed theoretical study of the effect of electron–electron interaction in quantum dots subjected to a perpendicular magnetic field was made by Maksym and Chakraborty.[25] The states of the interacting electrons in a parabolic quantum dot were calculated by numerically diagonalizing the many-electron Hamiltonian

$$\mathcal{H} = \sum_{nls} \mathcal{E}_{nl}\, c^{\dagger}_{nls}\, c_{nls} + \sum_{\substack{n_1 \ldots n_4 \\ l_1 \ldots l_4 \\ ss'}} \mathcal{A}_{n_1 l_1, n_2 l_2, n_3 l_3, n_4 l_4}\, c^{\dagger}_{n_1 l_1 s}\, c^{\dagger}_{n_2 l_2 s'}\, c_{n_3 l_3 s'}\, c_{n_4 l_4 s} \qquad (3)$$

where $\mathcal{A}$ is the Coulomb matrix element

$$\mathcal{A} = \frac{1}{2} \int d\mathbf{r}_1 d\mathbf{r}_2 \phi^*_{n_1 l_1}(\mathbf{r}_1) \phi^*_{n_2 l_2}(\mathbf{r}_2) V(\mathbf{r}_1 - \mathbf{r}_2) \phi_{n_3 l_3}(\mathbf{r}_2) \phi_{n_4 l_4}(\mathbf{r}_1),$$

where the Coulomb interaction is used for $V(\mathbf{r}_1 - \mathbf{r}_2)$.

In order to construct the basic states, the number of electrons n_e, total angular momentum $J = \Sigma l$ and the sum of Fock–Darwin level indices $\mathcal{N}_{\text{tot}} = \Sigma \mathcal{N}$ are first fixed. For example, for four

electrons, $J = 6$ and total Fock–Darwin level index $\mathcal{N}_{\text{tot}} = 0$ or $\mathcal{N}_{\text{tot}} = 1$, the basis consists of twelve states

$$a^{\dagger}_{n_1,l_1} a^{\dagger}_{n_2,l_2} a^{\dagger}_{n_3,l_3} a^{\dagger}_{n_4,l_4} |0\rangle,$$

where quantum numbers $(n_1, l_1)(n_2, l_2)(n_3, l_3)(n_4, l_4)$ have values for the lowest Fock–Darwin level ($\mathcal{N}_{\text{tot}} = 0$):

$$(0, 0) \quad (0, 1) \quad (0, 2) \quad (0, 3)$$

and for the second Fock–Darwin level ($\mathcal{N}_{\text{tot}} = 1$):

(0,0)	(0,1)	(0,2)	(1,3)	(0,−1)	(0,0)	(0,1)	(0,6)
(0,0)	(0,1)	(0,3)	(1,2)	(0,−1)	(0,0)	(0,2)	(0,5)
(0,0)	(0,1)	(0,4)	(1,1)	(0,−1)	(0,0)	(0,3)	(0,4)
(0,0)	(0,1)	(0,5)	(1,0)	(0,−1)	(0,1)	(0,2)	(0,4)
(0,0)	(0,2)	(0,3)	(1,1)	(0,1)	(0,2)	(0,3)	(1,0)
(0,0)	(0,2)	(0,4)	(1,0)				

The eigenstates of the system are the eigenstates of the total angular momentum J, which is conserved by the electron–electron interaction. The energy levels of the three- and four-electron system obtained numerically are shown in Fig. 11. For parameters appropriate to GaAs, the energies are plotted after subtracting $\hbar\Omega$ per electron. Clearly there are always two sets of broadened levels separated by a gap. In the limit of zero confinement potential these would be the lowest two Landau levels. The general trend is that energies increase with J because the single-electron energies increase with l.

The main difference between the high-field and low-field behavior is in the ground-state angular momentum. It is to be noted that the single-electron contribution increases linearly with J. In contrast, the interaction term decreases because electrons with higher angular momenta move in orbitals of larger radii, thereby decreasing the Coulomb energy. The net result is that the total energy as a function of J has a *minimum*. At low fields, this minimum occurs at the lowest available J, i.e., the smallest angular momentum compatible with placing the three or four electrons in

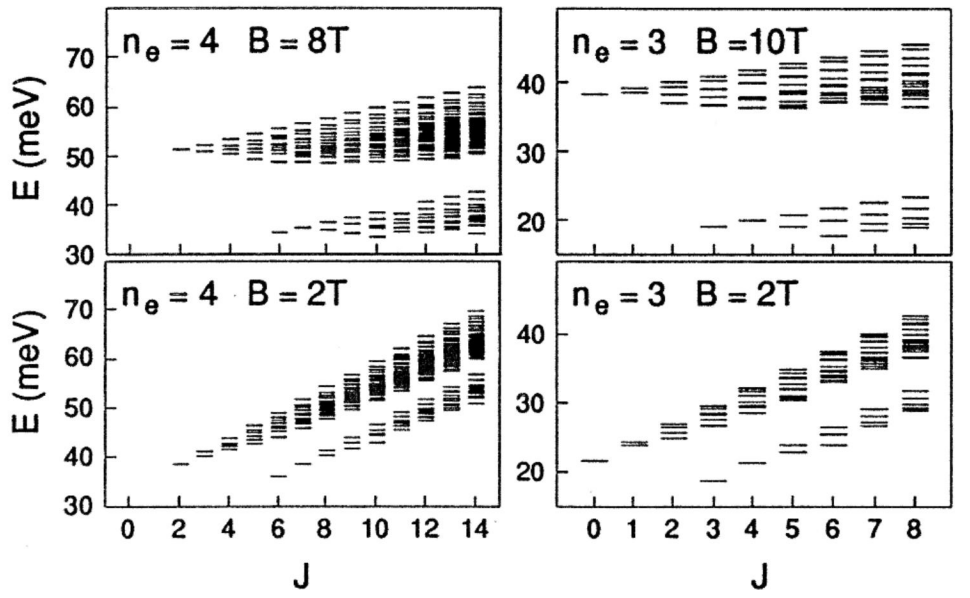

FIGURE 11 Energy levels as a function of J for three and four electrons in a parabolic quantum dot (Ref. 25).

$\mathcal{N} = 0$ states. At high fields, the minimum appears at a higher J value. The ground state of electrons in a magnetic field therefore occurs only at certain *magic* values[25] of the total angular momentum J. At these magic J values there are basis states in which electrons are kept very effectively. The ground state always occurs at one of these J values and the competition between interaction and confinement determines the optimum J.

The energy spectra of a two-electron system in a parabolic quantum dot were calculated by Merkt *et al.*,[26] and agree with the results discussed above.

C. Generalized Kohn's Theorem

The behavior of energy levels as a function of the magnetic field described above was not observed in FIR (or transport) spectroscopy. To understand this we have to consider the perturbation due to the electromagnetic radiation.[25] Typical wavelengths are 50 μm while typical dot sizes are 100 nm so the dipole approximation holds to a high degree of accuracy. This means that the perturbing Hamiltonian can be written in the form $\mathcal{H}' = \Sigma_{j=1}^{n_e} \mathbf{E}_0 \cdot \mathbf{r}_j \exp(-i\omega t)$, where $\mathbf{E}_0$ is the electric field and n_e is the electron number. This

can be expressed in terms of the center-of-mass coordinates (c.m.) $\mathbf{R} = \Sigma_i \mathbf{r}_i/n_e$ and the total charge $Q = n_e e$, i.e., $\mathcal{H}' = Q\mathbf{E}_0 \cdot \mathbf{R} \exp(-i\omega t)$. In the case of a parabolic confinement potential the many-electron Hamiltonian separates into terms which are functions of c.m. and relative coordinates. The c.m. Hamiltonian has exactly the same energy eigenvalues as those of a single confined electron because ω_c in the expression for $\mathcal{E}_{nl}$ depends only on the charge-to-mass ratio. As a result FIR absorption experiments observe only features at the single-electron energies when the confinement potential is parabolic.[25] Similar observations were also made by Bakshi *et al.*[27] A general derivation of this result is originally due to Brey, Johnson and Halperin[28] who proved that a parabolic quantum well absorbs FIR radiation at the bare harmonic-oscillator frequency independent of the electron–electron interaction and the number of electrons in the quantum well. To see this clearly, let us consider a Hamiltonian at zero magnetic field:

$$\mathcal{H} = \frac{1}{2m^*} \sum_{i=1}^{N} (p_{i,x}^2 + p_{i,y}^2 + p_{i,z}^2) + \sum_{i=1}^{N} \frac{1}{2} m^* \omega_0^2 z_i^2 + U \quad (4)$$

where $\mathbf{p}_i$ and $\mathbf{r}_i$ are the momentum and position operators of the i-th particle, ω_0 is the bare harmonic-oscillator frequency of the parabolic well, and $U = \Sigma_{i<j} u(\mathbf{r}_i - \mathbf{r}_j)$ is the interaction between electrons. Defining the raising and lowering operators

$$\hat{c}^{\pm} \equiv \sum_{i=1}^{N} (m^* \omega_0 z_i \mp i p_{i,z}),$$

we get

$$[\mathcal{H}, \hat{c}^{\pm}] = \pm \hbar \omega_0 \hat{c}^{\pm}.$$

This means that if ψ_n is an eigenstate of $\mathcal{H}$ with energy E_n,

$$\mathcal{H}\hat{c}^{\pm}\psi_n = (\pm \hbar \omega_0 + E_n)\, \hat{c}_{\pm}\psi_n.$$

If we define $\psi_{n\pm1} \equiv \hat{c}^{\pm}\psi_n$, then $\psi_{n\pm1}$ is an exact eigenstate of the Hamiltonian (4) with energy $E_{n\pm1} = E_n \pm \hbar\omega_0$.

In the presence of an electric field applied in the z direction, the interaction term to be added to the Hamiltonian is

$$\mathcal{H}' = \sum_{i=1}^{N} Ee^{-i\omega t} z_i = E \frac{e^{-i\omega t}}{2m^*\omega_0} (\hat{c}^+ + \hat{c}^-).$$

This perturbation connects ψ_N with the states $\psi_{N\pm1}$ only. The derivation was also extended to the case of a magnetic field by Brey *et al.* The result is, in fact, a generalization of Kohn's theorem[29] originally derived for the two-dimensional electron systems.

Dempsey *et al.*[30] studied the collective excitations in an array of parabolically confined quantum dots. Using instantaneous interactions and a harmonic approximation for the interdot interaction, they found that the Hamiltonian separates into a term that depends on the coupled c.m. motions of different dots and a term that depends on the relative coordinates within each dot. As expected, the light couples only to the c.m. modes. They also studied retardation effects which seem to reduce the dispersion of the c.m. modes in the optical region.

Although interesting, the above studies fail to provide any hint about how to observe the effect of the electron–electron interaction when the confinement potential is parabolic. One possible way is to engineer the dot such that the c.m. and the relative motions are coupled. The other is to study measurable thermodynamic properties such as the heat capacity.[31]

Heat Capacity

The electronic heat capacity C_v was calculated by Maksym and Chakraborty[25] from the temperature derivative of the mean energy. For simplicity, Landau level mixing is neglected. This does not, however, leave out any essential physics. The results for a three-electron system are shown in Fig. 12 for two different temperatures. For interacting electrons (solid lines) C_v is seen to be very different from that of noninteracting electrons (dotted lines). In the former case, C_v oscillates as a function of magnetic field B and has minima that are associated with crossovers from one ground

state J to another. The ground-state J is indicated by the dashed lines in Fig. 12. The origin of the oscillations is best understood by considering the curves for $T = 1$ K. At this low temperature the dominant contribution to C_v comes from two competing ground states. This causes the doublet structure around the crossovers and can be understood in terms of the magnetic field dependence of the gap between the corresponding ground states. Far away from a crossover, the gap is large, so C_v is small. Similarly, it is small exactly at a crossover because the gap in that case is zero. On either side of the crossover, the gap is nonzero but not too large. As a consequence C_v is nonzero because neither the probability of thermal excitation nor the associated heat absorption are vanishingly small.

Beyond Parabolic Confinement

Chakraborty, Halonen and Pietiläinen[32] considered a *pair* of quantum dots which are coupled only via the Coulomb interaction (tunneling of electrons between the dots was not allowed). This breaks the circular symmetry of a single dot and the dipole transition energies calculated for three- and four-electron dots as a function

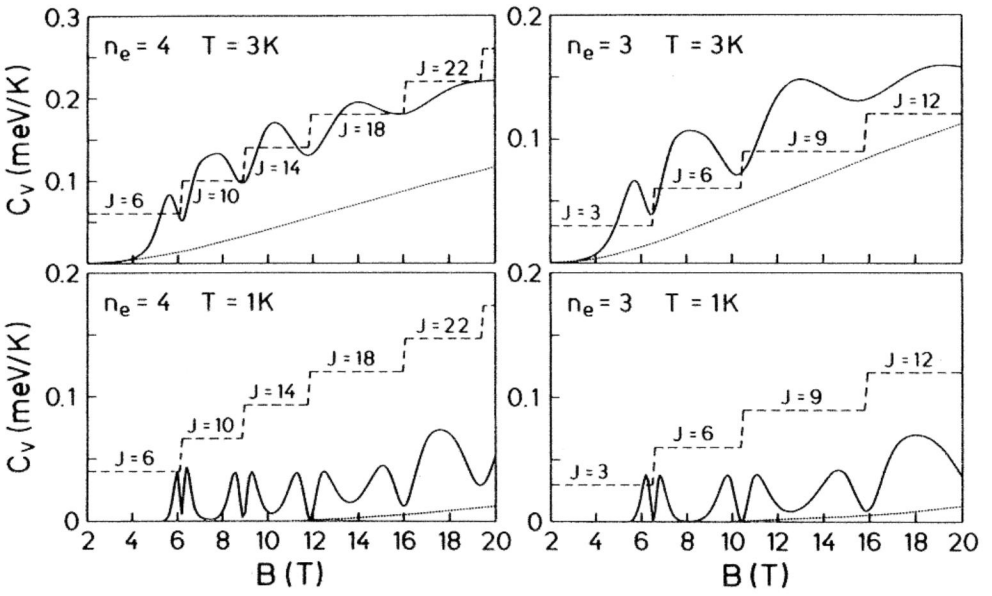

FIGURE 12 Electronic heat capacity C_v at two different temperatures and the ground-state J as a function of magnetic field for three electrons in a GaAs quantum dot (Ref. 25).

of B indeed showed anticrossing behavior somewhat similar to that observed experimentally by Demel *et al.*[5] One other interesting feature of the results was that, at $B = 0$, the degeneracy of the mode is lifted. This is due to breaking of the circular symmetry by the inter-dot Coulomb interaction. In fact, in a recent microwave response experiment on elliptic two-dimensional electron disks[33] the degeneracy of the resonance positions at $B = 0$ was found to have been lifted.

Gudmundsson and Gerhardts[34] considered a correction to the parabolic confinement potential by using $V_{\text{conf}} = ar^2 + br^4 + cr^6$ and various values for the constants a, b and c. In their numerical calculation, the ground state of the interacting electrons ($10 \leq n_e \leq 30$) in a dot was calculated in the Hartree approximation and the FIR response was treated in the random-phase approximation. A qualitative understanding of the experimental results by Demel *et al.*,[5] especially the appearance of the higher mode in the dispersion, was achieved in that work.

Pfannkuche and Gerhardts[35] studied the magneto-optical response to FIR radiation of quantum dots with two electrons (quantum-dot helium). They considered deviations from the parabolic confinement of the form: $U(\mathbf{r}) = \frac{1}{2} m^* \omega_4^2 (ar^4 + bx^2y^2)$ where ω_4, a, and b are constants. They found the splitting of the ω_+ mode and the mode coupling reflected in the anticrossing behavior of this mode.

D. Step Structures in the Magnetization

One other probe that is sensitive to the electron–electron interaction is the magnetization which can in principle be measured, e.g., Störmer *et al.*[36] have measured the magnetization of a 2DES. Theoretically it can be obtained by differentiating the energy eigenvalues with respect to the magnetic field. More precisely, the numerically generated eigenvalues (including spin) are used to compute the free energy which is then differentiated to get the magnetization.[37]

The results of such a calculation are shown in Fig. 13. The top panel of each figure gives the magnetization as a function of B, calculated both with and without interaction for (a) three electrons and (b) four electrons. The remaining panels show the ground

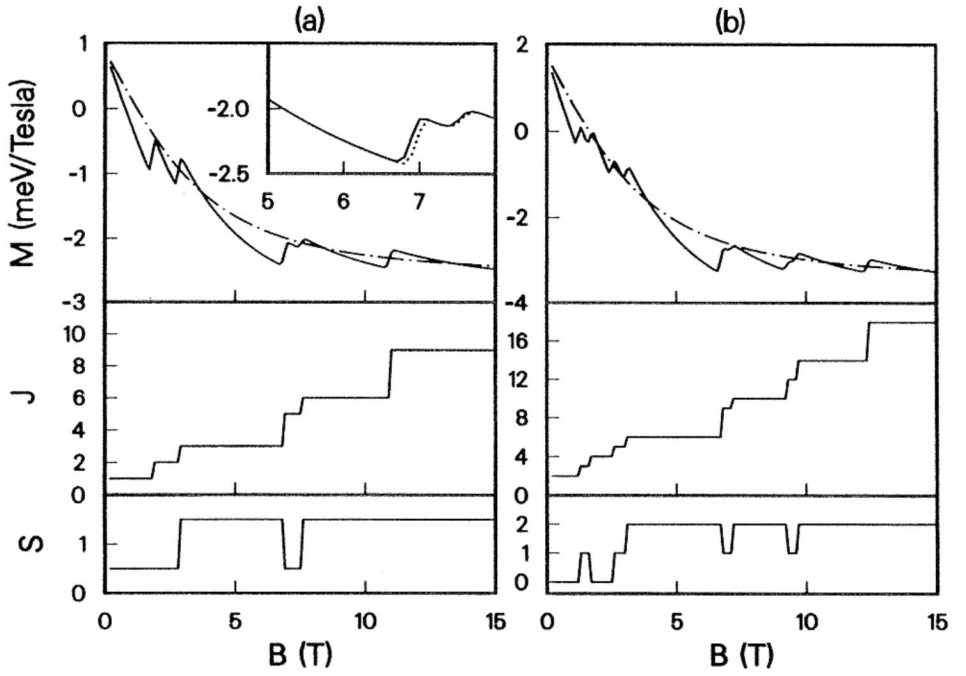

FIGURE 13 Magnetization $\mathcal{M}$ (meV/Tesla at $T = 0.1$ K of a parabolic quantum dot containing (a) three electrons ($\mathcal{N} = 1$), the ground state angular momentum J and the ground state spin S. The dash-dot line corresponds to the non-interacting case. A comparison of the results for the $\mathcal{N} = 2$ case (dotted line) is given in the inset and (b) four electrons per dot (Ref. 37).

state total angular momentum quantum number (J) and the ground state spin (S). All results are for GaAs quantum dots with $\hbar\omega_0 = 4$ meV. The calculations were done with the maximum value of $\mathcal{N}$ taken to be 1; that is, one electron was allowed to have $\mathcal{N} > 0$ and the other electrons had $\mathcal{N} = 0$. This truncation is surprisingly accurate, even at low magnetic fields. The absolute value of the magnetization is insensitive to the upper value of the $\mathcal{N}$ sum and the only effect of increasing it is that the positions of the steps change. This is illustrated in the inset of Fig. 13a where the results of allowing the upper limit of the $\mathcal{N}$ sum to rise to 2 are shown. Physically, the steps correspond to changes of the ground state J or both J and S, as can be seen by comparing the three panels of the figure.

The magnetization for non-interacting electrons has no step because the lowest two single-electron levels are unaffected by level crossings as the field is increased. Hence systems of up to four non-interacting electrons in the lowest spin state stay in the same

angular momentum state throughout the field range so the magnetization curve is smooth. All the steps in this case are a consequence of the interaction. For five or more non-interacting electrons the magnetization would be affected by negative l levels crossing positive l levels. However, the position of these crossings would be drastically affected by the interaction. In addition, there are relatively few of them when the electron number is small (for five electrons in the lowest spin state there is only one) and they tend to occur at low field. In contrast the steps due to the interaction occur at a regular sequence of J values throughout the field range.

Consider the simple case of a spin polarized system with electrons restricted to occupying $\mathcal{N} = 0$ states. In this case the expression for the total energy simplifies considerably because the interaction energy can be diagonalized independently of the confinement energy. In addition the confinement energy in this case is only a function of J so the total energy of each state takes the form

$$E = (n_e + J)\hbar\Omega - \frac{1}{2}J\hbar\omega_c + \frac{e^2}{\epsilon a}\lambda(J) + g^*\mu_B B S_z,$$

where the first two terms constitute the confinement energy, the third is the interaction energy (ϵ is the background dielectric constant) and the fourth is the Zeeman energy where $\lambda(J)$ is a dimensionless eigenvalue that depends only on J and g^* is the effective g-factor. For GaAs, g^* is small so the Zeeman term only affects the magnetization at the 1% level and the physics is determined by the first three terms. Differentiating them yields two contributions to magnetization:

$$\mathcal{M} = -\frac{\hbar e}{2m^*}\left[(J + n_e)\frac{\omega_c}{2\Omega} - J\right] - \frac{e^2}{2\epsilon}\frac{e}{\sqrt{\hbar m^*}}\frac{\omega_c}{(2\Omega)^{3/2}}\lambda(J).$$

These two terms behave very differently in the low and high field limits. When $B = 0$ the confinement term is $\hbar eJ/2m^*$, and as B increases it smoothly decreases and approaches $-\hbar en_e/2m^*$ as $B \to \infty$. In contrast the interaction term approaches 0 both when B

$\rightarrow 0$ and when $B \rightarrow \infty$. For the parameters used here this term contributes at the 1% level when $B < 2.5$ T and ~15% when $B = 10$ T. It is most significant when $2.5 < B \lesssim 10$ T. The field dependence of the magnetization at fixed J is essentially determined by the first term, and if J was independent of B the magnetization of the interacting system would be qualitatively similar to that of the non-interacting system. The major effect of the interaction is that the ground state J changes with magnetic field. Every time this happens the magnetization curve *shifts to a different track* and this causes the steps shown in Fig. 13. The effects of spin are important at fields $B \lesssim 10$ T; the system is spin polarized at higher fields. One effect of spin is that it causes extra steps in the magnetization. Each spin state has its own sequence of special J values, and each of those J values correspond to a possible ground state at that spin. As yet, no experimental attempts to measure either the heat capacity or the magnetization have been reported.

IV. FURTHER TOPICS

In this section, some interesting systems which are related to the studies of quantum dots are briefly discussed. The experimental work and the theoretical understanding of these systems are far less complete than those for the quantum dots. The aim of this section is to highlight their importance.

A. Excitons in a Parabolic Dot

A system of electrons and holes moving in two dimensions with their transverse motion quantized in the lowest Landau level and subjected to a strong perpendicular magnetic field is known to exhibit many interesting properties.[38–42] In the *ideal* case where the electron and hole wave functions are considered to be identical, Lerner and Lozovik[38] (and later Rice *et al.*[39]) found that the *exact* ground state is a Bose condensate of noninteracting magnetic excitons. Another interesting result found by Rice *et al.* was that there is no plasma oscillation in this system—a consequence of the confinement to the lowest Landau level. The collective excitation is simply given by the *single-exciton* dispersion relation which is a result of the ideal Bose character of the ground state.

Theoretical work by Bryant on excitons[43] and biexcitons[44] in

quantum boxes (in the absence of a magnetic field) demonstrated the competing effects of quantum confinement and Coulomb-induced electron–hole correlations. Excitons and biexcitons have also been studied recently in semiconductor microcrystallites by Koch *et al.*[45,46] It should be pointed out that the measurement of the exciton binding energy in the presence of a magnetic field has been reported in quantum wells[47] and quantum wires.[48] A brief review of the experimental work on excitons in quantum wires and dots can be found in Ref. 49.

Halonen, Chakraborty and Pietliäinen[50] have reported theoretical work on the properties of an exciton in a parabolic quantum dot in an external magnetic field using an effective mass Hamiltonian. They studied the ground state and low-lying excitation energies, electron–hole separation and the intensity for optical absorption. They predicted that from magneto-optical measurements one should be able to get the binding energy of the exciton and the strength of the confining potential. The problem certainly deserves more attention from both experimental and theoretical points of view.

B. Antidots

Antidots are reversed structures with respect to dots, i.e., where *holes are punched* into a 2DES at a regular interval. Ensslin and Petroff[51] and Weiss *et al.*[52] performed transport measurements on such systems and Kern *et al.*[53] studied them via FIR spectroscopy. The antidot samples of Kern *et al.* were prepared by deep-mesa-etching starting from the 2DES in a modulation-doped $Ga_xIn_{1-x}As/Al_yIn_{1-y}As$ single quantum well. A photoresist grid mask was prepared by holographic double exposure, and arrays of holes with typical diameters 100–300 nm were etched 100 nm deep into the buffer. The period in both lateral directions was $a = 300 - 400$ nm. A scanning micrograph of the antidot structure by Kern *et al.* is shown in Fig. 14a.

In the presence of a magnetic field, Kern *et al.* observed several resonances in the transmission spectra. The dispersion is shown in Fig. 14b for two antidot samples. The excitation spectrum has primarily two modes. The high-frequency mode, ω_+, first decreases in frequency and then increases with the magnetic field.

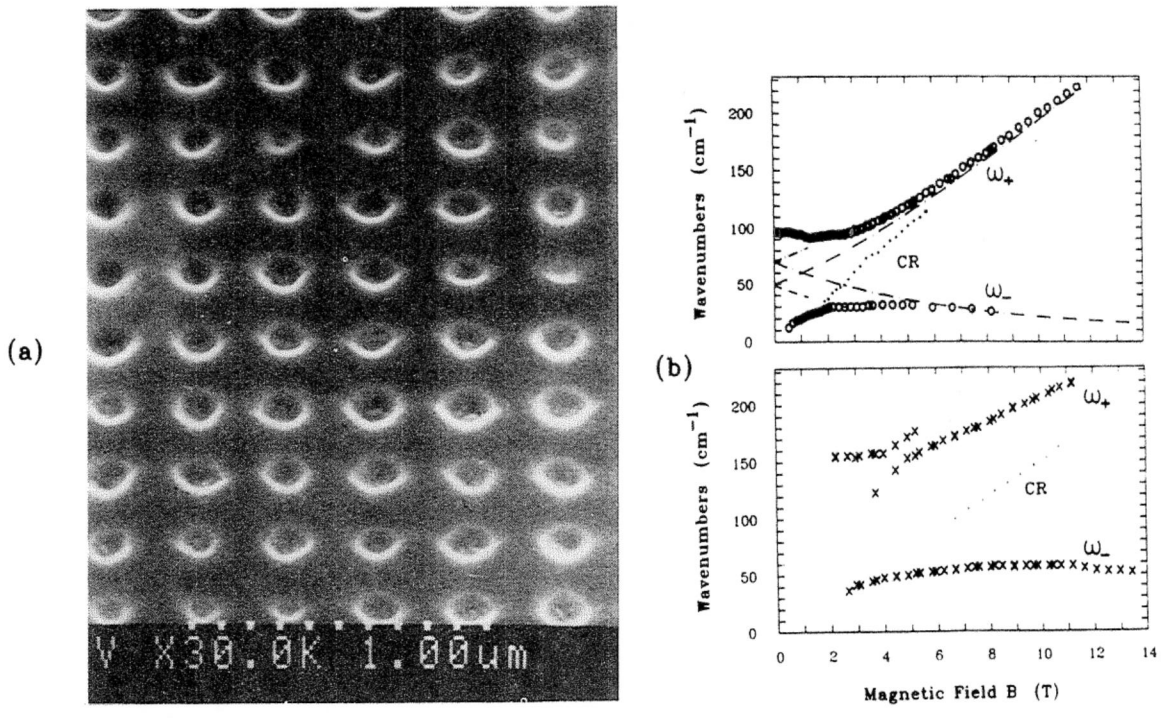

FIGURE 14 (a) Electron micrograph at an angle of 45° from an antidot array with a period $a = 300$ and holes of diameter of 300 nm etched into a GaInAs/AlInAs single quantum well. (b) Experimental dispersions of high- and low-frequency modes in two antidot samples. Upper panel: period 300 nm, hole diameter 200 nm and carrier density 8×10^{11}. Lower panel: same period but holes with smaller diameter 100 nm and a higher carrier density 2.5×10^{12}. CR corresponds to weak resonances near the Cyclotron resonance position. The dot-dashed lines are the results for the quantum dot case (Ref. 51).

At high B, it approaches the cyclotron frequency ω_c of the 2DES. The low-frequency mode, ω_-, follows ω_c and then bends down. The deviation from the quantum dot dispersion (dot-dashed line) is clearly visible in the low magnetic field region.

Detailed theoretical calculations of the antidot behavior are not yet available.

C. Quantum Rings

In recent work, van Houten *et al.*[54] suggested that when the electrons in a disk are in the lowest Landau level and when the charging energy is comparable to the cyclotron energy, the magnetoconductance oscillations are suppressed (*Coulomb blockage of the Aharonov–Bohm (AB) effect*). The blockage is lifted and the AB effect is recovered if one considers a *quantum ring* instead. In semiconductor nanostructures, quantum rings can be created from a two-dimensional electron system with an additional gate within the gates shaping the disk (quantum dot) (see Section IIC). Application of a negative voltage to this additional gate would deplete the central region of the disk, thereby forming a ring. In the lowest Landau level the basic difference between the two systems is the behavior of the electrochemical potential (or the energy cost associated with the addition of a single electron to the disk or the ring) as a function of the magnetic field which determines the conductance oscillations. The situation is different when the second Landau level is occupied, in which case the electrochemical potential for a dot has the same *sawtooth* behavior as that for a ring and the Coulomb blockage of the AB effect, as discussed above, is lifted[54]—a situation exploited in the experiment of McEuen *et al.*[17]

The ring geometry is also very useful to study various other phenomena, e.g., periodic oscillation of thermodynamic quantities like the magnetization in weak[55] and strong magnetic fields,[56] as a function of the magnetic flux and observation of the persistent currents[57,58] (which is related to the periodic nature of the free energy), etc. Also, in the quantum Hall regime, Halperin[15] employed it to demonstrate the importance of the *edge states* in quantizing the Hall conductivity.

The Hamiltonian for an electron confined in a parabolic ring and subject to a magnetic field is given by[59]

$$\mathcal{H} = \frac{1}{2m^*}\left(\mathbf{p} - \frac{e}{c}\mathbf{A}\right)^2 + \frac{1}{2}m^*\omega_0^2(r - r_0)^2$$

where the vector potential is $\mathbf{A} = \frac{1}{2}(-By, Bx, 0)$ (symmetric gauge). Introducing the quantities[18,54]

$$N_s = \frac{\Phi}{\Phi_0} = \frac{BeA}{hc}, \quad \alpha = \frac{\omega_0 m^* A}{h}$$

where A is the area of the ring, $A = \pi r_0^2$ and $\Phi_0 = hc/e$ is the flux quantum, the radial part of the Schrödinger equation is written as

$$f'' + \frac{1}{x}f' + \left[4\lambda + 2N_s l - 4\alpha^2 - (N_s^2 + 4\alpha^2)x^2 + 8\alpha^2 x - \frac{l^2}{x^2}\right] f = 0. \quad (5)$$

Here we have introduced the dimensionless quantities, $x = r/r_0$ and $\lambda = (2m^*\pi A/h^2)E$. As a check, let us consider the case of δ-function confinement, i.e., set $x = 1$. Equation (5) then has the solution $\lambda = \frac{1}{4}(N_s - l)^2$. This case was originally studied by Büttiker *et al.*[57] and is shown in Fig. 15(a).

In Fig. 15(b)–(d), we have also plotted the single-electron energy levels for the parabolic ring for various values of α (α is inversely proportional to the width of the ring). The results are obtained by numerically solving Eq. (5). As α decreases, i.e., the ring becomes wider, the *sawtooth* behavior of the narrow ring is gradually replaced by the formation of the Landau levels.

Unlike the case of the quantum dot, magnetization and susceptibilities show periodic oscillations even in the absence of electron–electron interactions. These oscillations are gradually damped at high fields for wider rings, reflecting the behavior of the energy

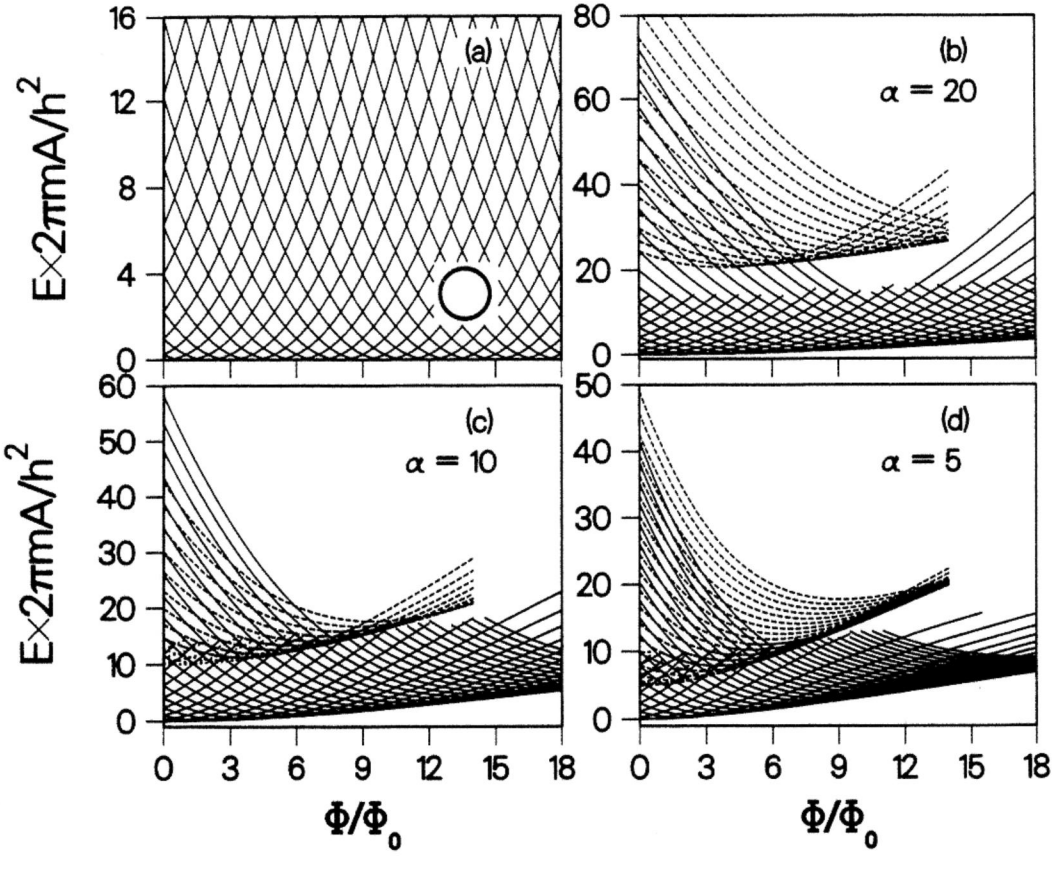

FIGURE 15 (a) Single-electron energy levels as a function of B for (a) narrow ring and (b)–(d) wide parabolic quantum rings with various values of the confinement potential strength. The second Fock–Darwin level is plotted as dotted lines.

levels discussed above. The influence of the Coulomb interaction on these quantities is an important problem and is currently under investigation.[60]

V. CONCLUDING REMARKS

Since the first experiments on quantum dots in a magnetic field in 1989, the field has witnessed very rapid growth. At present, theoretical work is no match for the volume of raw data available from the experiments and the data are still coming in! Of course, the theoretical results are no less interesting. In fact, the aim of this Comment is partly to make theorists aware of the experimental results that need to be understood. The results on antidots (*electron pinball*) and transport measurements on quantum dots are the present challenges for theorists while the theoretical results for the magnetization, excitons in quantum dots and for quantum rings should invite some experimental activity. The physics of artificial atoms will be an open book for a long time to come.

Acknowledgments

I wish to acknowledge fruitful collaboration on these and other topics with Peter Maksym (Leicester, UK), Pekka Pietiläinen and Veikko Halonen (Oulu, Finland). I have learned a great deal about this subject from Detlef Heitmann and Klaus von Klitzing at the Max-Planck-Institute, Stuttgart, and Ulrich Merkt (Hamburg) and would like to thank them. I am indebted to Peter Fulde for his support and encouragement. I would like to thank Geof Aers for critically reading this manuscript.

TAPASH CHAKRABORTY
Institute for Microstructural Sciences,
National Research Council,
Montreal Road, M-50,
Ottawa, Canada K1A 0R6

References

1. U. Merkt, Advances in Solid State Physics **30**, 77 (1990).
2. T. P. Smith III, Surf. Sci. **229**, 239 (1990).

3. W. Hansen, T. P. Smith III, K. Y. Lee, J. A. Brum, C. M. Knoedler, J. M. Hong and D. P. Kern, Phys. Rev. Lett. **62**, 2168 (1989).
4. W. Hansen, T. P. Smith III, K. Y. Lee, J. M. Hong and C. M. Knoedler, Appl. Phys. Lett. **56**, 168 (1990).
5. D. C. Tsui, H. L. Störmer and A. C. Gossard, Phys. Rev. Lett. **48**, 1559 (1982); Tapash Chakraborty and P. Pietiläinen, *The Fractional Quantum Hall Effect* (Springer-Verlag, New York, Berlin, Heidelberg, 1988).
6. Ch. Sikorski and U. Merkt, Phys. Rev. Lett. **62**, 2164 (1989); Surf. Sci. **229**, 282 (1990); *Spectroscopy of Semiconductor Microstructures,* eds. G. Fasol, A. Fasolino and P. Lugli, NATO ASI Series B: Physics, Vol. 206 (Plenum, New York, 1989).
7. T. Demel, D. Heitmann, P. Grambow and K. Ploog, Phys. Rev. Lett. **64**, 788 (1990).
8. D. Heitmann, B. Meurer, T. Demel, P. Grambow and K. Ploog, *Proceedings of the Workshop on Intersubband Resonances in Quantum Wells, Cargese, France, 1991.*
9. K. Kern, T. Demel, D. Heitmann, P. Grambow, Y. H. Zhang and K. Ploog, Superlattices and Microstructures **9**, 11 (1991).
10. B. Meurer, D. Heitmann and K. Ploog, preprint (1991).
11. A. Lorke, J. P. Kotthaus and K. Ploog, Phys. Rev. Lett. **64**, 2559 (1990).
12. C. W. J. Beenakker and H. van Houten, Solid State Physics **44**, 1 (1991).
13. H. van Houten, C. W. J. Beenakker and A. A. M. Staring, *Single Charge Tunneling,* eds. H. Grabert and M. H. Devoret, NATO ASI Series B (Plenum, New York, 1991).
14. B. J. van Wees, L. P. Kouwenhoven, K. J. P. M. Harmans, J. G. Williamson, C. E. Timmering, M. E. I. Broekaart, C. T. Foxon and J. J. Harris, Phys. Rev. Lett. **62**, 2523 (1989); L. P. Kouwenhoven, B. J. van Wees, K. J. P. Harmans and J. G. Williamson, Surf. Sci. **229**, 290 (1990).
15. B. I. Halperin, Phys. Rev. B **25**, 2185 (1982).
16. R. P. Taylor, A. S. Sachrajda, J. A. Adams, P. Zawadski, P. T. Coleridge and M. Davies, unpublished.
17. P. L. McEuen, E. B. Foxman, U. Meirav, M. A. Kastner, Y. Meir, N. S. Wingreen and S. J. Wind, Phys. Rev. Lett. **66**, 1926 (1991).
18. C. W. J. Beenakker, H. van Houten and A. A. M. Staring, Phys. Rev. B **44**, 1657 (1991); A. A. M. Staring, J. G. Williamson, H. van Houten, C. W. J. Beenakker, L. P. Kouwenhoven and C. T. Foxon, Physica B **175**, 226 (1991).
19. A. Kumar, S. E. Laux and F. Stern, Phys. Rev. B **42**, 5166 (1990).
20. V. Fock, Z. Physik **47**, 446 (1928).
21. C. G. Darwin, Proc. Cambridge Philos. Soc. **27**, 86 (1930).
22. L. Landau, Z. Physik **64**, 629 (1930).
23. R. B. Dingle, Proc. R. Soc. London, Ser. A **212**, 38 (1952).
24. G. W. Bryant, Phys. Rev. Lett. **59**, 1140 (1987).
25. P. A. Maksym and Tapash Chakraborty, Phys. Rev. Lett. **65**, 108 (1990).
26. U. Merkt, J. Huser and M. Wagner, Phys. Rev. B **43**, 7320 (1991).
27. P. Bakshi, D. A. Broido and K. Kempa, Phys. Rev. B **42**, 7416 (1990).
28. L. Brey, N. F. Johnson and B. I. Halperin, Phys. Rev. B **40**, 10, 647 (1989); see also, F.M. Peeters, Phys. Rev. B **42**, 1486 (1990).
29. W. Kohn, Phys. Rev. **123**, 1242 (1961).
30. J. Dempsey, N. F. Johnson, L. Brey and B. I. Halperin, Phys. Rev. B **42**, 11708 (1990).
31. E. Gornik, R. Lassnig, G. Strasser, H. L. Störmer, A. C. Gossard and W. Wiegmann, Phys. Rev. Lett. **54**, 1820 (1985).

32. Tapash Chakraborty, V. Halonen and P. Pietiläinen, Phys. Rev. B **43**, 14, 289 (1991).
33. C. Dahl, F. Brinkop, A. Wixforth, J. P. Kotthaus, J. H. English and M. Sundaram, Solid State Comm. **80**, 673 (1991).
34. V. Gudmundsson and R. R. Gerhardts, Phys. Rev. B **43**, 12, 098 (1991).
35. D. Pfannkuche and R. R. Gerhardts, Phys. Rev. B **44**, 13, 132 (1991).
36. T. Haavasoja, H. L. Störmer, D. J. Bishop, V. Narayanamurti, A. C. Gossard and W. Wiegmann, Surf. Sci. **142**, 294 (1984); J. P. Eisenstein, H. L. Störmer, V. Narayanamurti, A. Y. Cho, A. C. Gossard and C. W. Tu, Phys. Rev. Lett. **55**, 875 (1985).
37. P. A. Maksym and Tapash Chakraborty, Phys. Rev. B **45** (1992); see also, M. Wagner, U. Merkt and A. V. Chaplik, preprint (1991), for a two-electron calculation.
38. I. V. Lerner and Yu. E. Lozovik, Zh. Eksp. Teor. Fiz. **80**, 1448 (1981) [Sov. Phys. JETP **53**, 763 (1981)].
39. T. M. Rice, D. Paquet and K. Ueda, Phys. Rev. B **32**, 5208 (1985); Helv. Phys. Acta **58**, 410 (1985).
40. C. Kallin and B. I. Halperin, Phys. Rev. B **30**, 5655 (1984).
41. L. P. Gorkov and I. E. Dzyaloshinskii, Zh. Eksp. Teor. Fiz. **53**, 717 (1967) [Sov. Phys. JETP **26**, 449 (1968)].
42. M. Shinada and S. Sugano, J. Phys. Soc. Jpn. **21**, 1936 (1966); O. Akimoto and H. Hasegawa, *ibid.* **22**, 181 (1967); M. Shinada and K. Tanaka, *ibid.* **29**, 1258 (1970).
43. G. W. Bryant, Phys. Rev. B **37**, 8763 (1988); Surf. Sci. **196**, 596 (1988).
44. G. W. Bryant, Phys. Rev. B **41**, 1243 (1990).
45. Y. Z. Hu, M. Lindberg and S. W. Koch, Phys. Rev. B **42**, 1713 (1990).
46. Y. Z. Hu, S. W. Koch, M. Lindberg, N. Peyghambarian, E. L. Pollock and F. A. Abraham, Phys. Rev. Lett. **64**, 1805 (1990); E. L. Pollock and S. W. Koch, J. Chem. Phys. **94**, 6776 (1991).
47. J. C. Maan, G. Belle, A. Fasolino, M. Altarelli and K. Ploog, Phys. Rev. B **30**, 2253 (1984); D. C. Rogers, J. Singleton, R. J. Nicholas, C. T. Foxon and K. Woodbridge, Phys. Rev. B **34**, 4002 (1986); W. Ossau, B. Jäkel, E. Bangert, G. Landwehr and G. Weimann, Surf. Sci. **174**, 188 (1986).
48. M. Kohl, D. Heitmann, P. Grambow and K. Ploog, Phys. Rev. Lett. **63**, 2124 (1989).
49. K. Kash, J. Luminescence **46**, 69 (1990).
50. V. Halonen, Tapash Chakraborty and P. Pietiläinen, Phys. Rev. B (to be published).
51. K. Ensslin and P. M. Petroff, Phys. Rev. B **41**, 12, 307 (1990).
52. D. Weiss, M. L. Roukes, A. Menschig, P. Grambow, K. von Klitzing and G. Weimann, Phys. Rev. Lett. **66**, 2790 (1991).
53. K. Kern, D. Heitmann, P. Grambow, Y. H. Zhang and K. Ploog, Phys. Rev. Lett. **66**, 1618 (1991).
54. C. W. J. Beenakker, H. van Houten and A. A. M. Staring, *Granular Nanoelectronics*, eds. D. K. Ferry, J. Barker and C. Jacobini (Plenum, New York, 1991).
55. E. N. Bogacheck and G. A. Gogadze, JETP **36**, 973 (1973).
56. U. Sivan and Y. Imry, Phys. Rev. Lett. **61**, 1001 (1988).
57. M. Büttiker, Y. Imry and R. Landauer, Phys. Lett. A **96**, 365 (1983).
58. V. Chandrasekhar, R. A. Webb, M. J. Brady, M. B. Ketchen, W. J. Gallagher and A. Kleinsasser, Phys. Rev. Lett. **67**, 3578 (1991).
59. Tapash Chakraborty and P. Pietiläinen, *Proc. of the 14th Taniguchi International Symposium on Physics of Mesoscopic Systems, Shima, Japan, Nov. 11–14, 1991* (Springer-Verlag, 1992)(to be published).
60. P. Pietiläinen and Tapash Chakraborty, preprint (1992).